ALBERT-LUDWIGS-UNIVERSITÄT FREIBURG
INSTITUT FÜR INFORMATIK
Lehrstuhl für Mustererkennung und Bildverarbeitung

The Connection of Shape Distributions and Haar Integrals

Internal Report 3/05

Marco Reisert

April 2005

The Connection of Shape Distributions and Haar Integrals

Marco Reisert
Computer Science Department
Albert-Ludwigs-University Freiburg
79110 Freiburg, Germany
reisert@informatik.uni-freiburg.de

March, 2005

1 Introduction

In this technical report we want to connect two invariant feature extraction techniques, namely Shape Distribution and feature extraction based on Group Integration. Both techniques have a proven good performance, where Group Integration is mainly used for feature extraction on gray-value images [5, 6, 7, 1] and Shape Distributions have their application area in 3D Shape Retrieval [4, 3].

To show the connection we formulate the feature extraction process in continuous space by introducing the notion of fill- and binning-functions. We also establish an interesting connection of the Shape Distribution to the rotational averaged Power spectrum, i.e. the squared magnitudes of Fourier Transform averaged over concentric spheres around the origin in fourier domain. We will see that both are equivalent in an unitary sense.

The presented theoretical insights give us more intuition how already known invariant features extraction techniques are related and show that most of them are theoretically equivalent in a linear sense. We will also give a small set of experiments, which also prove our results empirically.

2 Establishing the Connection

The Shape $\mathbf{S} \subset \mathbb{R}^3$ is given by a measurable subset of $\mathbb{R}^3$. Thinking of 3D surface models the shape is the set of points on the surface of the model. A continous gray-value image is a volumetric function $f : \mathbb{R}^3 \mapsto \mathbb{R}$.

2.1 Shape Distribution revisited

A D_2 Shape Distribution [4] measures how often two points on a surface of an object appear within some distance α. It can be written by a double integral as follows

$$D_2(\alpha) = \int_{\mathbf{x}\in\mathbf{S}} \int_{\mathbf{y}\in\mathbf{S}} h_\alpha(||\mathbf{x}-\mathbf{y}||)\; d\mu(\mathbf{x})\; d\mu(\mathbf{y})$$

where $h_\alpha : \mathbb{R} \mapsto \mathbb{R}$ is a binning-function, which gives contribution whenever its argument is nearby α. By $d\mu(\mathbf{x})$ we denote an appropriate measure element of the shape (usually a surface element).

2.2 Haar integrals based on second-order Monoms

Group Integration features average some nonlinear kernel-function over the considered group. The appropriate group measure is known as the Haar-measure. The typical second-order monomial Haar-Integral for a function $f : \mathbb{R}^3 \mapsto \mathbb{R}$ is given by

$$H_2(\alpha) = \int_{\mathbf{s}\in S^2_\alpha} \int_{\mathbf{u}\in\mathbb{R}^3} f(\mathbf{u}) f(\mathbf{u}-\mathbf{s})\; d\mathbf{u}\; d\mu(\mathbf{s}) \tag{1}$$

where S^2_α denotes a sphere with radius α and $d\mu(\mathbf{s})$ the corresponding area element. Those features were successfully applied in [5]. A shape can be represented by a function $f_\mathbf{S} : \mathbb{R}^3 \mapsto \mathbb{R}$ as follows

$$f_\mathbf{S}(\mathbf{u}) = \int_{\mathbf{x}\in\mathbf{S}} g(\mathbf{u}-\mathbf{x})\; d\mu(\mathbf{x}) \tag{2}$$

where $g : \mathbb{R}^3 \mapsto \mathbb{R}$ is a isotropic 'fill'-function like a Gaussian or something else. This embedding is nothing else than a convolution of the shape represented by Dirac-Distributions with the 'fill'-function.

2.3 Merging them

Now let us show how the connection between the Haar Integral H_2 applied on $f_\mathbf{S}$ and the Shape Distribution D_2 applied on $\mathbf{S}$ can be established. First we insert (2) in (1) and rearrange the integration

$$\int_{\mathbf{x}\in\mathbf{S}} \int_{\mathbf{y}\in\mathbf{S}} \left[\int_{\mathbf{s}\in S^2_\alpha} \int_{\mathbf{u}\in\mathbb{R}^3} g(\mathbf{u}-\mathbf{x}) g((\mathbf{u}-\mathbf{s})-\mathbf{y})\; d\mathbf{u}\; d\mu(\mathbf{s}) \right] d\mu(\mathbf{x})\; d\mu(\mathbf{y}) \tag{3}$$

Now we shift the integration variables, which we can do since the integration ranges over the whole domain. We rename the inner integral with

$$G(\mathbf{x}-\mathbf{y}-\mathbf{s}) = \int_{\mathbf{u}\in\mathbb{R}^3} g(\mathbf{u}) g(\mathbf{u}+\mathbf{x}-\mathbf{y}-\mathbf{s})\; d\mathbf{u},$$

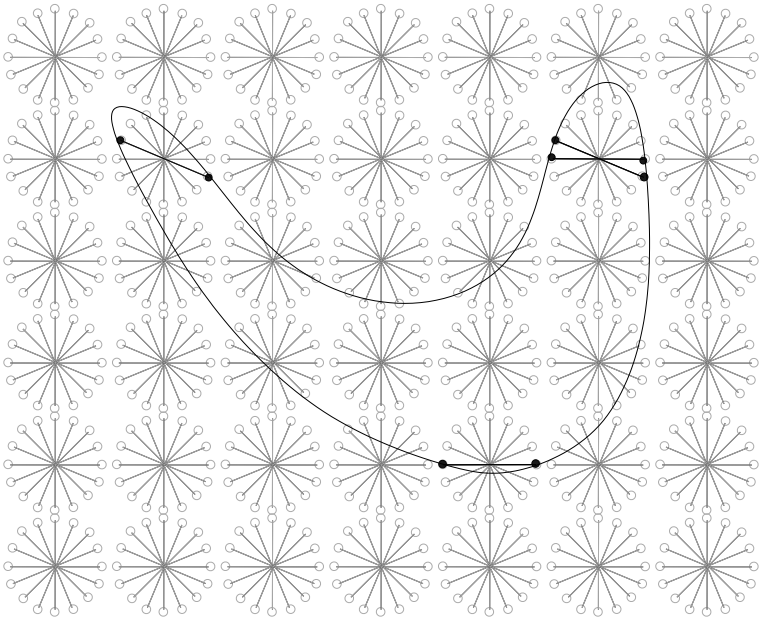

Figure 1: Moving two points in all translational and orientational poses over the object and count how often both points hit the surface of the model.

where G is actually the autocorrelation of g. Rewriting expression (3) gives

$$\int_{\mathbf{x}\in\mathbf{S}} \int_{\mathbf{y}\in\mathbf{S}} \left[\int_{\mathbf{s}\in S^2_\alpha} G(\mathbf{x}-\mathbf{y}-\mathbf{s})\, d\mu(\mathbf{s}) \right] d\mu(\mathbf{x})\, d\mu(\mathbf{y})$$

where we can identify the integral over the sphere S^2_α with the binning function h_α, which we introduced above. We have the correspondence

$$h_\alpha(||\mathbf{x}-\mathbf{y}||) = \int_{\mathbf{s}\in S^2_\alpha} G(\mathbf{x}-\mathbf{y}-\mathbf{s})\, d\mu(\mathbf{s}).$$

The RHS necessarily depends only on the norm of $\mathbf{x}-\mathbf{y}$, because the only rotation-invariant feature of a point is its distance from the rotation center, and the integral over the sphere generates this invariance.

The result that D_2 Shape Distribution and H_2 Haar Integrals are the same is also very intuitive. If we imagine the shape as the function we have already explained, a function which gives contribution whenever its argument is on the surface of the object. If we now move two points with some fix distance α in all orientation and all translational poses over the shape, multiply the values of the function at those points and sum everything up, we obtain nothing else than a 2^{nd} order monom over the Euclidean group. And it is obvious that such an integral counts how often two points on the surface of the model occur in a distance α. In Figure 1 we give an illustration of this procedure.

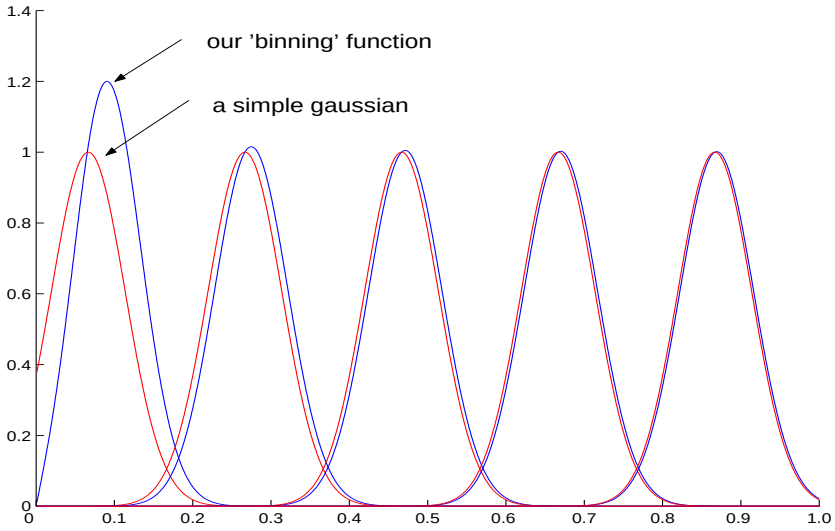

Figure 2: Comparing a Gaussian binning function to the one obtained in (4).

2.4 Gaussian 'Fill'-functions

Now we go into detail and examine how the 'binning'-function looks if we assume a Gaussian fill functions. We have

$$g(\mathbf{u}) = e^{-\frac{||\mathbf{u}||^2}{\sigma^2}}$$

and hence we get for the autocorrelation

$$G(\mathbf{u}) = c\, e^{-\frac{||\mathbf{u}||^2}{2\sigma^2}}.$$

where c is some constant, i.e. autocorrelation is just a broader Gaussian. Following the general way from the last section we arrive after some calculation at

$$h_\alpha(\beta) = c' \frac{\alpha}{\beta}(e^{-\frac{(\beta-\alpha)^2}{2\sigma^2}} + e^{-\frac{(\beta+\alpha)^2}{2\sigma^2}}). \tag{4}$$

Unfortunately this binning-function is not shift-invariant, i.e. it does not hold $h_\alpha(\beta) = h_{\alpha+\gamma}(\beta+\gamma)$. But this property should be expected from a usual binning-function. But if we have a closer look for large α,β shift-invariance is approximately fulfilled. Only nearby zero we get into trouble. In Figure 2 we compare a simple Gaussian 'binning'-function to the one obtained above. If the centers α of the function are far away (relative to the width σ) from zero the function in (4) is nearly a Gaussian, only for small α the differences get large. Of course, the smaller we choose the width σ, the less differences we get for a fixed value of α.

2.5 Extension to higher orders

The results from Section 2.3 are easily extended to higher order monoms, i.e. any group integral over the Euclidean transformation group of the form

$$\int_{SO(3)} \int_{\mathbf{t}\in\mathbb{R}^3} f(\mathbf{R}\mathbf{u}_1 + \mathbf{t}) ... f(\mathbf{R}\mathbf{u}_n + \mathbf{t})\, d\mathbf{R} d\mathbf{t}$$

can be written as integrals over the shape

$$\int_{\mathbf{S}\times ...\times \mathbf{S}} h_{(\mathbf{u}_1,...,\mathbf{u}_n)}(\mathbf{s}_1, ...\mathbf{s}_n)\, d\mu(\mathbf{s}_1) ... d\mu(\mathbf{s}_n),$$

where h is a generalized 'binning'-function again depending on the 'fill'-function. We know that h is invariant to Euclidean motion in the sense that

$$h_{(\mathbf{R}\mathbf{u}_1+\mathbf{t},...,\mathbf{R}\mathbf{u}_n+\mathbf{t})} = h_{(\mathbf{u}_1,...,\mathbf{u}_n)}.$$

This statement also includes that in the case of second-order monoms the binning-function h only depends on the norm $||\mathbf{u}_1 - \mathbf{u}_2||$ which we formerly called α.

3 The Connection to the Power Spectrum

In the following we establish the connection of D_2 and H_2 to the fourier spectrum of the shape. Rewriting equation (1) we obtain

$$H_2(\alpha) = \int_{\mathbf{u}\in\mathbb{R}^3} f(\mathbf{u}) \left[\int_{\mathbf{s}\in S^2_\alpha} f(\mathbf{u}-\mathbf{s})\, d\mu(\mathbf{s}) \right] d\mathbf{u} \tag{5}$$

$$= \int_{\mathbf{u}\in\mathbb{R}^3} f(\mathbf{u}) \left[\int_{\mathbf{u}'\in\mathbb{R}^3} f(\mathbf{u}-\mathbf{u}')\delta(||\mathbf{u}'|| - \alpha)\, d\mathbf{u}' \right] d\mathbf{u} \tag{6}$$

We can identify the inner integral with a convolution of the function f with a sphere of radius α and we can write

$$H_2(\alpha) = \int_{\mathbf{u}\in\mathbb{R}^3} f(\mathbf{u})\, [f * B_\alpha](\mathbf{u})\, d\mathbf{u} \tag{7}$$

where $*$ denotes the convolution and we used $B_\alpha(\mathbf{u}) = \delta(||\mathbf{u}|| - \alpha)$, where B_α is just a function representing a sphere around the origin with radius α. The Fourier Transform is known to be a very powerful tool when dealing with convolution, so we reformulate (7) in fourier space and get

$$H_2(\alpha) = \int_{\mathbf{k}\in\mathbb{R}^3} |\widetilde{f}(\mathbf{k})|^2\, \widetilde{B_\alpha}(\mathbf{k})\, d\mathbf{k}, \tag{8}$$

where $\widetilde{\cdot}$ denotes the Fourier Transform. One can derive that the Fourier Transform of a sphere is related to the *sinc*-function as follows

$$\widetilde{B_\alpha}(\mathbf{k}) = 4\pi\alpha^2\, \mathrm{sinc}(\alpha||\mathbf{k}||)$$

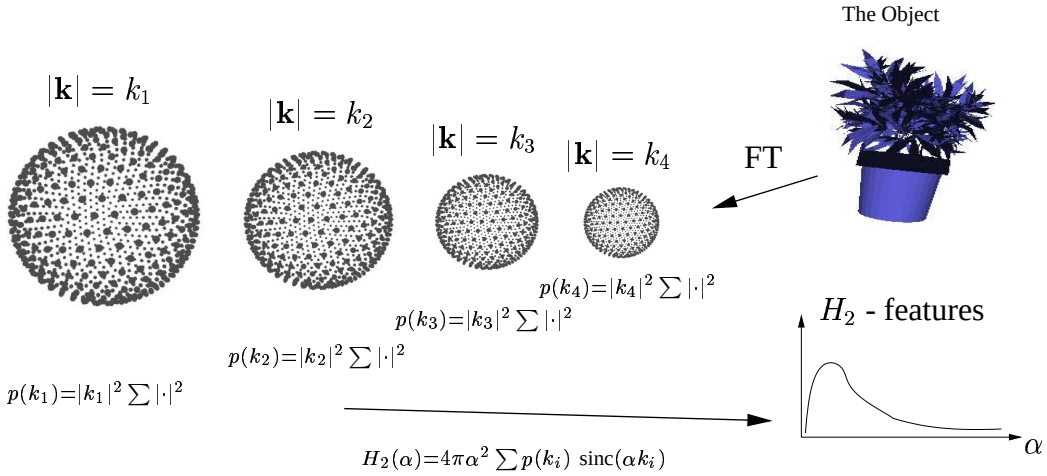

Figure 3: Explanation of the algorithm

Since $\widetilde{B_\alpha}(\mathbf{k})$ is a isotropic function we can perform the angular integration in (8) independently and get

$$H_2(\alpha) = 4\pi\alpha^2 \int_0^\infty p(k)\ \mathrm{sinc}(\alpha k)\ dk \tag{9}$$

where $p(k)$ is squared magnitude of $\widetilde{f}(\mathbf{k})$ averaged over a sphere of radius k, i.e.

$$p(k) = \int_{\mathbf{k}\in S_k^2} |\widetilde{f}(\mathbf{k})|^2 d\mu(\mathbf{k}) \tag{10}$$

We established the connection between H_2 and D_2 respectively to the power spectrum $p(k)$. And it is actually the case that in theory equation (9) is one to one. One can derive that

$$p(k) = 2k^2 \int_0^\infty H_2(\alpha)\ \mathrm{sinc}(\alpha k)\ d\alpha$$

with appropriate 'fill'- and binning-functions. We can conclude, if D_2 or H_2 are given we are able to compute $p(k)$ and backwards.

4 Experiments

In this Section we shortly explain an algorithm to compute H_2 in fourier space. We show that for 3D surface models our theoretical results can be empirically verified.

4.1 Implementation

We first compute the averaged magnitude of the fourier spectrum following equation (10). We do this by a Monte Carlo approach. First we compute the fourier

transform

$$\widetilde{f}(\mathbf{k}) = \sum_{\mathbf{p} \in Rnd(\mathbf{S})} e^{-\mathbf{i}\mathbf{k}\cdot p - \mathbf{k}^2/\sigma^2},$$

where used Gaussian fill-functions. The wave-vectors $\mathbf{k}$ are chosen equidistributed and deterministically on a sphere with appropriate radii $k = |\mathbf{k}|$. In the experiments 282 points were distributed over the sphere [2] by an energy-minimizing approach. The set $Rnd(\mathbf{S})$ stands for some randomly chosen points on the surface of the model. To obtain those points we followed the approach by Osada [4]. For every different $\mathbf{k}$, of course, new random points were chosen. The size of $Rnd(\mathbf{S})$ is 1000 in the experiments. The fourier coefficent were calculated for 128 different radii k, i.e. we computed $128 * 282 = 36096$ fourier coefficients. After that, the computation of $p(k)$ is straight-forward. The last step to obtain H_2 is to compute an approximation of (9). We did this without any interpolation scheme, just by substituting the integral by a discrete sum. In Figure 3 we illustrate the method. For the implementation of D_2 we completely follow the algorithm proposed in [4].

4.2 Empirical Verification

In Figure 4 we give two examples for the computation method proposed above. One can see that both methods give nearly the same results, which gives an empirical verification of our theoretical results. The computation of H_2 is about 1.5 seconds on an *Intel P4 2.8Ghz*, of course D_2 is faster to compute (0.5 seconds), since there is no intermediate representation of the features in fourier domain.

5 Conclusion

We have given theoretical insights how two different invariant feature extraction methods, which are known from two different fields of pattern recognition, are related. We have also proven by a small experiment that the theory also holds in practice. The introduced theory is also able to connect the Haar-integral features with features proposed by Ohbuchi [3] which also use surface-normals to compute the histograms. In this case the scalar 'fill'-function we introduced here would be extended to a vector-valued fill-function.

References

[1] B. Haasdonk, A. Halawani, and H. Burkhardt. Adjustable invariant features by partial haar-integration. In *Proceedings of the 17th International Conference on Pattern Recognition (ICPR)*, volume 2, pages 769–774, 2004.

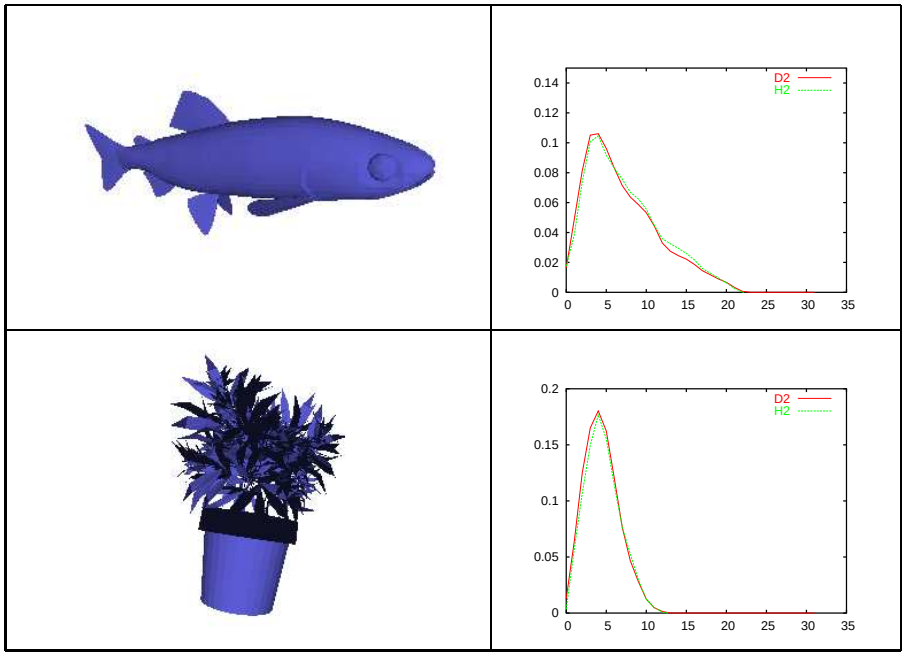

Figure 4: Comparison of D_2 and H_2.

[2] R. Hardin, W. Smith, and N. Sloane. *Spherical Codes*. Information Sciences Research AT&T Shannon Lab Florham Park, NJ 07932-0971 *www.research.att.com/ njas/*, 2000.

[3] R. Ohbuchi, T. Minamitani, and T. Takei. Shape-similarity search of 3d models by using enhanced shape functions. *International Journal of Computer Applications in Technology (IJCAT)*, 23:70–85, 2005.

[4] Robert Osada, Thomas Funkhouser, and Bernard Chazelle und David Dobkin. Matching 3d models with shape distribution. In *Proceedings Shape Modeling International*, 2001.

[5] O. Ronneberger, H. Burkhardt, and E. Schultz. General-purpose Object Recognition in 3D Volume Data Sets using Gray-Scale Invariants. In *Proceedings of the International Conference on Pattern Recognition*, Quebec, Canada, September 2002.

[6] Hanns Schulz-Mirbach. *Anwendung von Invarianzprinzipien zur Merkmalgewinnung in der Mustererkennung*. PhD thesis, TU Hamburg Harburg, February 1995. Reihe 10, Nr. 372, VDI-Verlag.

[7] S. Siggelkow and H. Burkhardt. Improvement of histogram-based image retrieval and classification. In *Proceedings of the International Conference on Pattern Recognition*, volume 3, pages 367–370, 2002.